



香港城市大學  
City University of Hong Kong

專業 創新 胸懷全球  
Professional · Creative  
For The World

## CityU Scholars

### Optical fiber drawing and dopant transport

Huang, H.; Miura, R. M.; Wylie, J. J.

**Published in:**

SIAM Journal on Applied Mathematics

**Published:** 01/01/2008

**Document Version:**

Final Published version, also known as Publisher's PDF, Publisher's Final version or Version of Record

**Publication record in CityU Scholars:**

[Go to record](#)

**Published version (DOI):**

[10.1137/070700176](https://doi.org/10.1137/070700176)

**Publication details:**

Huang, H., Miura, R. M., & Wylie, J. J. (2008). Optical fiber drawing and dopant transport. *SIAM Journal on Applied Mathematics*, 69(2), 330-347. <https://doi.org/10.1137/070700176>

**Citing this paper**

Please note that where the full-text provided on CityU Scholars is the Post-print version (also known as Accepted Author Manuscript, Peer-reviewed or Author Final version), it may differ from the Final Published version. When citing, ensure that you check and use the publisher's definitive version for pagination and other details.

**General rights**

Copyright for the publications made accessible via the CityU Scholars portal is retained by the author(s) and/or other copyright owners and it is a condition of accessing these publications that users recognise and abide by the legal requirements associated with these rights. Users may not further distribute the material or use it for any profit-making activity or commercial gain.

**Publisher permission**

Permission for previously published items are in accordance with publisher's copyright policies sourced from the SHERPA RoMEO database. Links to full text versions (either Published or Post-print) are only available if corresponding publishers allow open access.

**Take down policy**

Contact [lbscholars@cityu.edu.hk](mailto:lbscholars@cityu.edu.hk) if you believe that this document breaches copyright and provide us with details. We will remove access to the work immediately and investigate your claim.



## OPTICAL FIBER DRAWING AND DOPANT TRANSPORT\*

H. HUANG<sup>†</sup>, R. M. MIURA<sup>‡</sup>, AND J. J. WYLIE<sup>§</sup>

**Abstract.** Optical fibers are made of glass with different refractive indices in the (inner) core and the (outer) cladding regions. The difference in refractive indices arises due to a rapid transition in the concentration of a dopant across the boundary between these two regions. Fibers are normally drawn from a heated glass preform, and the different dopant concentrations in the two regions will change due to dopant diffusion and convective transport induced by the flow. In this paper, we analyze a mathematical model for the dynamics of dopant concentration changes during the fiber drawing process. Using a long-wave approximation, we show that the governing equations can be reduced to a simple diffusion equation. As a result, we are able to identify key dimensionless parameters that contribute to the diffusion process. We also derive asymptotic solutions for the temperature, cross-sectional area, and effective diffusion coefficient when there are strong temperature dependencies in the viscosity and the diffusion coefficient. Our simplified model and asymptotic solutions reduce the need for extensive numerical simulations and can be used to devise control strategies to limit excess dopant diffusion.

**Key words.** dopant diffusion, optical fiber drawing, incompressible viscous flow, long-wave approximation, asymptotic approximation

**AMS subject classifications.** 76D99, 76R50, 41A60, 76D27

**DOI.** 10.1137/070700176

**1. Introduction.** Optical fibers are drawn from a heated glass preform using mechanical pullers. The glass preform is fabricated so that there is a difference in the refractive index between the fiber core and the outer cladding region. This refractive index difference is achieved normally by adding a dopant to the inner core region [4]. Typically, dopant materials, such as oxides of germanium, phosphorus, and boron, are deposited in pure silica in the preform. However, during drawing, splicing, and fusion, the refractive index may change due to diffusion of the dopant in the glass [7, 11].

Compared to dopant concentration changes due to splicing and fusion of these fibers, dopant concentration changes during fiber drawing would appear to be more complicated since dopant diffusion depends not only on temperature, but also on a number of other factors, including the mechanics of the drawing process. In Lytikäinen et al. [5], numerical simulations and an experimental study of specialized fibers have been carried out. For relatively low drawing speeds, it was shown that diffusion can cause a small but visible spreading of the dopant. It also was shown that larger drawing speeds and lower furnace temperatures both reduce the diffusion of dopant. Their simulations ignored advection of dopant by the flow and were based

---

\*Received by the editors August 14, 2007; accepted for publication (in revised form) July 23, 2008; published electronically October 29, 2008.

<http://www.siam.org/journals/siap/69-2/70017.html>

<sup>†</sup>Department of Mathematics and Statistics, York University, Toronto, ON M3J 1P3 Canada (hhuang@yorku.ca). This author was supported by NSERC and MITACS of Canada and by the Programme of Introducing Talents of Discipline to Universities of China (18 B08018).

<sup>‡</sup>Department of Mathematical Sciences, New Jersey Institute of Technology, Newark, NJ 07102 (miura@njit.edu). This author was supported by the Division of Mathematical Sciences at NSF (0709092).

<sup>§</sup>Department of Mathematics, City University of Hong Kong, Kowloon, Hong Kong (mawylie@cityu.edu.hk). This author was supported by a grant from the Research Grants Council of the Hong Kong Special Administrative Region, China (CityU 103207).

on a simple diffusion equation with only a radial component. Their experiments and simulations compare favorably, which indicates that the key mechanism is captured by simple radial diffusion; however, it is not clear why this is the case and whether this assumption will hold for other parameter values. On the other hand, Yan and Pitchumani [11] carried out a full numerical simulation of the drawing process, including dopant diffusion. Although the fiber surface is a free boundary, they simplified their computations by using a prescribed surface boundary based on previous numerical studies of the drawing process by Lee and Jaluria [6]. Contrary to the conclusion in Lyytikäinen et al. [5], the numerical simulations by Yan and Pitchumani [11] show that a significant amount of diffusion occurs during the drawing process, in spite of a similar drawing environment and higher drawing speeds, which should reduce the amount of diffusion.

In this paper, we analyze a mathematical model for dopant concentration changes during optical fiber drawing. The main objective of the paper is to understand the mechanism of dopant transport during drawing. We also are interested in exploring different ways to control dopant diffusion since from a practical point of view it is desirable to minimize its effect. Based on an asymptotic analysis of this model, we are able to show that the diffusion of dopant is governed by a simple diffusion equation with only a radial component, as used by Lyytikäinen et al. [5]. However, the molecular diffusion coefficient used in [5] must be replaced by an effective diffusion coefficient, which includes a “history” factor. For typical parameter values, we show that the effective diffusion coefficient is determined mainly by two dimensionless parameters, namely, the Péclet number based on the diffusion coefficient for dopant, and a parameter that quantifies the heating strength. For large changes in viscosity, we derive analytical expressions that are uniformly valid asymptotic expansions for velocity, radius, and temperature. This allows us to find simple expressions for the effective diffusion coefficient that clearly show the way in which all of the parameters affect the diffusion process and hence reduces the need for extensive numerical simulations.

The paper is organized as follows. In section 2, the mathematical model for glass optical fiber drawing is given and subsequently simplified. We derive explicit approximations for the temperature and cross-sectional area in section 3. For these approximations, we considered two cases, one with cooling and one without cooling. In section 4, we derive asymptotic approximations for the effective diffusion in the case of no cooling.

**2. Problem description.** In a typical setup for glass optical fiber drawing, a cylindrical preform with radius  $R_0$  and temperature  $T_0$  is extruded from an input nozzle into a heating and cooling device with speed  $u_0$ ; see Figure 1. At a distance  $L$  from the input nozzle, the fiber is pulled out of the device by a roller. Between the input nozzle and a distance  $L_f < L$ , the fiber is inside a furnace and is subjected to heating. This heating causes the viscosity of the glass to dramatically decrease, and thus facilitates rapid stretching of the fiber with moderate forces. Between the end of the furnace and the roller, the fiber is cooled by natural and forced cooling. At the nozzle input, the dopant concentration  $c = c_0(r)$  will be assumed to be a given function of the radial distance from the fiber axis,  $r$ . The aim of this study is to understand how the heating, cooling, and the stretching process, as well as the diffusion and advection of the dopant, affect the dopant concentration profile when the fiber exits the device. We note that throughout this paper, subscripts 0,  $f$ , and  $c$  refer to quantities associated with the input nozzle, furnace heating, and cooling, respectively.

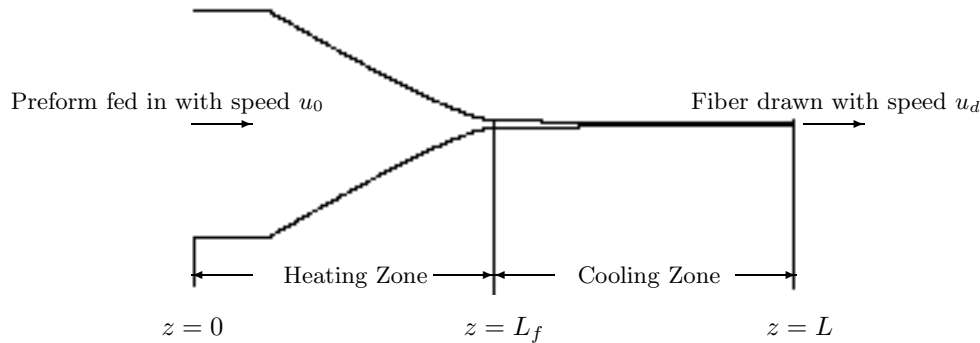


FIG. 1. Schematic of heating and cooling zones.

**2.1. Mathematical model.** We assume that the glass fiber is an incompressible fluid with temperature-dependent viscosity. Also, we assume that the dopant concentration has a negligible effect on the density, viscosity, and conductivity of the glass, the fiber remains axisymmetric, and the drawing conditions are in a steady state. Under these assumptions, the governing equations for mass, momentum, energy, and dopant concentration are given by [11]

$$(2.1) \quad \frac{\partial(\rho u)}{\partial z} + \frac{1}{r} \frac{\partial(r\rho v)}{\partial r} = 0,$$

$$(2.2) \quad \frac{\partial(\rho u^2)}{\partial z} + \frac{1}{r} \frac{\partial(r\rho uv)}{\partial r} = -\frac{\partial p}{\partial z} + 2\frac{\partial}{\partial z} \left( \mu \frac{\partial u}{\partial z} \right) + \frac{1}{r} \frac{\partial}{\partial r} \left[ r\mu \left( \frac{\partial u}{\partial r} + \frac{\partial v}{\partial z} \right) \right],$$

$$(2.3) \quad \frac{\partial(\rho uv)}{\partial z} + \frac{1}{r} \frac{\partial(r\rho v^2)}{\partial r} = -\frac{\partial p}{\partial r} + \frac{\partial}{\partial z} \left[ \mu \left( \frac{\partial u}{\partial r} + \frac{\partial v}{\partial z} \right) \right] + \frac{2}{r} \frac{\partial}{\partial r} \left( r\mu \frac{\partial v}{\partial r} \right) - \frac{2\mu v}{r^2},$$

$$(2.4) \quad \frac{\partial(\rho c_p u T)}{\partial z} + \frac{1}{r} \frac{\partial(r\rho c_p v T)}{\partial r} = \frac{\partial}{\partial z} \left( k \frac{\partial T}{\partial z} \right) + \frac{1}{r} \frac{\partial}{\partial r} \left( r k \frac{\partial T}{\partial r} \right),$$

$$(2.5) \quad \frac{\partial(\rho u c)}{\partial z} + \frac{1}{r} \frac{\partial(r\rho v c)}{\partial r} = \frac{\partial}{\partial z} \left( D \frac{\partial c}{\partial z} \right) + \frac{1}{r} \frac{\partial}{\partial r} \left( r D \frac{\partial c}{\partial r} \right),$$

where  $z$  is the distance from the input nozzle measured along the axis of the fiber,  $u$  and  $v$  are the velocity components in the axial and radial directions, respectively,  $p$  is the pressure,  $T$  is the temperature,  $c$  is the dopant concentration,  $\rho$  is the density,  $\mu$  is the viscosity,  $c_p$  is the specific heat,  $k = k_T + k_R$  is the effective conductivity [11] where  $k_T$  is the (molecular) thermal conductivity and  $k_R$  is the radiative conductivity, and  $D$  is the molecular diffusivity of the dopant. We observe that the mass, momentum, and energy equations decouple from the dopant equation.

The boundary conditions at the inlet of the furnace are

$$(2.6) \quad u = u_0, \quad v = 0, \quad T = T_0, \quad c = c_0(r), \quad 0 \leq r \leq R_0, \quad \text{at } z = 0.$$

At a fixed downstream location, we assume the velocity is known:

$$(2.7) \quad u = u_d \quad \text{at } z = L.$$

At this downstream location, boundary conditions also are needed for the radial component of the velocity  $v$ , the temperature  $T$ , and the dopant concentration  $c$ . However, we will show that in the asymptotic limit of the long-wave approximation, such

boundary conditions do not play a significant role outside of a thin region near this boundary. The lateral fiber surface  $r = R(z)$  is a free boundary at which the following dynamic and kinematic conditions must be applied:

$$(2.8) \quad \mathbf{n}^T \cdot \boldsymbol{\sigma} \cdot \mathbf{n} = \Gamma \kappa, \quad \mathbf{t}^T \cdot \boldsymbol{\sigma} \cdot \mathbf{t} = 0, \quad v = R' u$$

where the prime denotes differentiation with respect to  $z$ ,  $\boldsymbol{\sigma}$  is the stress tensor,  $\mathbf{n} = [(1 + R'^2)^{-1/2}, R'(1 + R'^2)^{-1/2}]^T$  is the outward normal vector to the glass surface,  $\mathbf{t} = [-R'(1 + R'^2)^{-1/2}, (1 + R'^2)^{-1/2}]^T$  is the corresponding vector in the tangential direction,  $\kappa$  is the mean curvature, and  $\Gamma$  is the surface tension coefficient.

The boundary condition for temperature at the fiber surface depends on whether the fiber is inside or outside of the furnace. In Lee and Jaluria [6], the heat flux  $q$  is specified when the fiber is inside the furnace. In general,  $q$  depends on many factors, such as the furnace wall temperature profile, inert gas flow, and the dimensions of the furnace, as well as the fiber temperature. Here, as in previous studies [6], we have adopted the standard Newton's cooling law<sup>1</sup>

$$(2.9) \quad -k \frac{\partial T}{\partial n} = q := \begin{cases} h_f(T_f - T), & 0 \leq z < L_f, \\ -h_c(T - T_c), & L_f \leq z \leq L, \end{cases}$$

where  $T_f$  and  $T_c$  are the furnace and background temperatures, respectively, and  $h_f$  and  $h_c$  are the heat transfer coefficients for the heating from the furnace and cooling to the background, respectively. For simplicity, we will assume that the background temperature is the same as the temperature at the nozzle input, that is,  $T_c = T_0$ , although generalization is straightforward.

Finally, the dopant concentration satisfies the no-flux boundary condition

$$(2.10) \quad D \frac{\partial c}{\partial n} = 0$$

at the fiber surface  $r = R(z)$  and the regularity condition

$$(2.11) \quad \frac{\partial c}{\partial r} = 0$$

at the axis of the fiber  $r = 0$ .

For the glass fibers used in typical optical fiber fabrication, the viscosity of the fiber varies rapidly with temperature. This rapid variation plays a fundamental role in controlling the dynamics. Empirical data for glass (see [8, 3] and the references therein) show that the viscosity can be well approximated by an Arrhenius formula or an exponential law. In this paper, we will use the exponential law in the form

$$(2.12) \quad \mu(T) = \mu_0 \exp(-G_\mu(T - T_0))$$

where  $\mu_0$  is the viscosity of the fiber at  $T_0$  and  $G_\mu$  is a constant. The diffusion coefficient for the dopant also is normally assumed to follow the Arrhenius formula

$$(2.13) \quad D(T) = D_\infty \exp\left(-\frac{G_D}{T}\right)$$

where  $G_D$  is the activation energy divided by the universal gas constant and  $D_\infty$  is the diffusion coefficient at high temperatures.

<sup>1</sup>Within the furnace, there is a complicated balance between radiative and convective heat processes, but it is straightforward to generalize our approach, as outlined in this paper, to heating laws for these processes, e.g., for radiative heat transfer; see [3].

TABLE 1  
List of the physical parameter values.

$\rho$ kg/m <sup>3</sup>	$c_p$ J/(K kg)	$k_T$ W/(m K)	$k_R$ W/(m K)	$\Gamma$ kg/s	$h_f$ W/(m <sup>2</sup> K)	$h_c$ W/(m <sup>2</sup> K)
$2.23 \times 10^3$	$7.538 \times 10^2$	1.130	$1.2 \times 10^1$	$3 \times 10^{-1}$	200	20

$u_0$ m/s	$u_d$ m/s	$L$ m	$L_f$ m	$R_0$ m	$T_0$ K	$T_f$ K	$\mu_0$ kg/(m s)	$G_\mu$ K <sup>-1</sup>	$D_\infty$ m <sup>2</sup> /s	$G_D$ K
$10^{-4}$	1	0.5	0.1	$6 \times 10^{-3}$	300	2300	$10^8$	$2 \times 10^{-2}$	$2.4 \times 10^{-6}$	$3.73 \times 10^4$

**2.2. Dimensional analysis.** We nondimensionalize the governing equations using the following scalings:

$$\hat{z} = \frac{z}{L}, \quad \hat{r} = \frac{r}{R_0}, \quad \hat{R} = \frac{R}{R_0}, \quad \hat{u} = \frac{u}{u_0}, \quad \hat{v} = \frac{Lv}{R_0 u_0}, \quad \hat{p} = \frac{R_0^2 p}{\mu_0 u_0 L},$$

$$\hat{\mu} = \frac{\mu}{\mu_0}, \quad \theta = \frac{T - T_0}{T_f - T_0}, \quad \hat{c}_0 = \frac{c_0}{c_0(0)}, \quad \hat{c} = \frac{c}{c_0(0)}, \quad \hat{D} = \frac{D}{D_\infty}.$$

Substitution of these scalings into (2.1)–(2.4) yields the following dimensionless parameters, which we list along with their order of magnitude estimates based on the typical parameter values [5, 6, 11] that are listed in Table 1:

$$D_r = \frac{u_d}{u_0} \approx 10^4, \quad \delta = \frac{R_0}{L} \approx 10^{-2}, \quad \text{Re} = \frac{\rho u_0 L}{3\mu_0} \approx 10^{-9}, \quad \lambda = \frac{\Gamma L}{3\mu_0 u_0 R_0} \approx 10^{-3},$$

$$\text{Bi} = \frac{h_f R_0}{k} \approx 10^{-1}, \quad \alpha_\mu = G_\mu(T_f - T_0) \approx 40, \quad \alpha_D = \frac{G_D}{T_f - T_0} \approx 20,$$

$$\Theta = \frac{T_0}{T_f - T_0} \approx 0.15, \quad \mathcal{P} = \frac{u_0 R_0^2}{L D_\infty} \approx 3 \times 10^{-3},$$

and

$$\mathcal{H}_f = \frac{2\sqrt{\pi} h_f L}{\rho c_p u_0 R_0} \approx 350, \quad \mathcal{H}_c = \frac{2\sqrt{\pi} h_c L}{\rho c_p u_0 R_0} \approx 35, \quad \ell = \frac{L_f}{L} \approx 0.2.$$

Here  $D_r$  is the draw ratio,  $\delta$  is the aspect ratio,  $\text{Re}$  is the Reynolds number,  $\lambda$  is the ratio of surface tension forces to viscous forces, and  $\text{Bi}$  is the Biot number. The parameters  $\alpha_\mu$  and  $\alpha_D$  measure the changes in the viscosity and the diffusion coefficient as the temperature varies between its initial value and the heater temperature, respectively,  $\Theta$  is the ratio of the initial temperature to the difference between the heater and initial temperatures,  $\mathcal{P}$  is the Péclet number for the dopant,  $\mathcal{H}_f$  and  $\mathcal{H}_c$  represent the dimensionless strengths of the heating and cooling, respectively, and  $\ell$  represents the proportion of the length of the device that is heated by the furnace. We note that the Biot number estimated here is consistent with the value cited in [6], where the heat transfer is estimated based on an estimate for the heat flux.

**2.2.1. Flow and temperature equations: Simplifications.** The mass, momentum, and temperature equations clearly decouple from the dopant equation, and we begin by simplifying these equations. Based on the parameter values given in Table 1, we see that  $\delta$ ,  $\text{Re}$ ,  $\lambda$ , and  $\text{Bi}$  are small. Since  $\delta \ll 1$ , we can use the long-wave approximation. Furthermore, since  $\lambda \ll 1$  and  $\text{Re} \ll 1$ , we can ignore the inertia and

surface tension terms in the momentum equations. Finally, assuming that  $Bi \ll 1$ , equations (2.1)–(2.4) become (dropping the hats)

$$(2.14) \quad \frac{\partial}{\partial z}(us) = 0,$$

$$(2.15) \quad \frac{1}{s} \frac{\partial}{\partial z} \left( \mu s \frac{\partial u}{\partial z} \right) = 0,$$

$$(2.16) \quad u \frac{\partial \theta}{\partial z} = \frac{\mathcal{H}_f(1 - \theta)H(\ell - z) - \mathcal{H}_c\theta H(z - \ell)}{s^{1/2}},$$

where  $s = R^2$ ,  $\mu = \exp(-\alpha_\mu\theta)$ , and  $H$  is the Heaviside step function. The derivation of these equations follows the derivation of similar equations in previous work (cf. [1, 2, 9, 10]).

The boundary conditions (2.6) and (2.7) become

$$(2.17) \quad s = 1, u = 1, \theta = 0 \quad \text{at} \quad z = 0$$

and

$$(2.18) \quad u = D_r \quad \text{at} \quad z = 1.$$

**2.2.2. Dopant equation: Long-wave approximation.** The long-wave approximation of the dopant concentration equation (2.5) is

$$(2.19) \quad \mathcal{P} \left( u \frac{\partial c}{\partial z} - \frac{r}{2} \frac{\partial u}{\partial z} \frac{\partial c}{\partial r} \right) = \frac{1}{r} \frac{\partial}{\partial r} \left( r D \frac{\partial c}{\partial r} \right)$$

where

$$(2.20) \quad D = \exp \left( -\frac{\alpha_D}{\theta + \Theta} \right).$$

The boundary conditions are

$$(2.21) \quad c = c_0(r), \quad 0 \leq r \leq R_0, \quad \text{at} \quad z = 0$$

and

$$(2.22) \quad c_r = 0 \quad \text{at} \quad r = 0 \quad \text{and} \quad r = \sqrt{s}.$$

**2.2.3. Flow and temperature equations: Reduced system.** From (2.14), (2.15), and the boundary conditions on  $u$  and  $s$  in (2.17) and (2.18), it is easy to verify that

$$(2.23) \quad su = 1 \quad \text{and} \quad \mu s u_z = 2F$$

where

$$F = \frac{\ln D_r}{2 \int_0^1 \mu^{-1} dz}$$

is the effective pulling force that will be obtained by using the boundary condition at  $z = 1$ . Using the first equation in (2.23) to eliminate  $u$  in the temperature equation



(2.16) and  $u_z$  in the second equation in (2.23), we obtain a system of two coupled first-order ordinary differential equations for  $s$  and  $\theta$ :

$$(2.24) \quad s_z = -\frac{2Fs}{\mu},$$

$$(2.25) \quad \theta_z = s^{1/2} [\mathcal{H}_f(1-\theta)H(\ell-z) - \mathcal{H}_c\theta H(z-\ell)],$$

which must be solved subject to the following boundary conditions:

$$(2.26) \quad s = 1, \theta = 0 \quad \text{at} \quad z = 0 \quad \text{and} \quad s = D_r^{-1} \quad \text{at} \quad z = 1.$$

**2.2.4. Dopant equation: Simplification.** We can further simplify the equation for dopant concentration changes by defining

$$(2.27) \quad \phi(z) \equiv \int_0^z D[\theta(z')]dz' \quad \text{and} \quad \bar{\phi} \equiv \phi(1)$$

and using the coordinate transformations  $\xi = r/R$  and  $\tau = \phi(z)/\bar{\phi}$ . The quantity

$$(2.28) \quad \mathcal{D} = \frac{\bar{\phi}}{\mathcal{P}}$$

will be called the effective diffusion coefficient, and we obtain

$$(2.29) \quad c_\tau = \frac{\mathcal{D}}{\xi} \frac{\partial}{\partial \xi} \left( \xi \frac{\partial c}{\partial \xi} \right)$$

subject to

$$(2.30) \quad c = c_0(\xi) \quad \text{at} \quad \tau = 0$$

and

$$(2.31) \quad c_\xi = 0 \quad \text{at} \quad \xi = 0 \quad \text{and} \quad \xi = 1.$$

The exit of the entire heating and cooling device is located at  $\tau = 1$ .

To summarize, we have shown that dopant transport during fiber drawing is governed by a diffusion equation in the coordinates  $(\xi, \tau)$ , which has the form for diffusion in cylindrically symmetric heat flow. The amount of diffusion is characterized by the effective diffusion coefficient,  $\mathcal{D}$ , which depends on the temperature distribution inside the fiber. In principle, the fiber temperature can be obtained by solving two coupled first-order ordinary differential equations (2.24) and (2.25) numerically. The effective diffusion coefficient can then be evaluated numerically using (2.27).

Since the range of temperature variation is large, the value of the molecular diffusion coefficient varies over several orders of magnitude and the effective diffusion coefficient is mainly determined by the portion of the fiber where the temperature is high. It can be seen that if the temperature is uniformly high, i.e.,  $\theta = \text{constant}$ , then  $\bar{\phi} = D(\theta)$  and  $\mathcal{D} = D(\theta)/\mathcal{P}$ . Therefore, to estimate the value of the effective diffusion coefficient, it is important to obtain an estimate of the temperature inside the fiber. In the next two sections, we show that due to special features of the setup and parameter values used in practice, approximate solutions could be obtained for the fiber temperature. In the case without cooling, solutions also can be obtained for the effective diffusion coefficient. When compared with numerical solutions, such asymptotic solutions provide valuable insights for understanding the dopant transport mechanism.

**3. Asymptotic solution for  $\theta$  and  $s$ .** We consider two cases: first without cooling ( $\ell = 1$ ), in which the furnace heats the entire fiber, followed by the case with cooling ( $\ell < 1$ ), in which the furnace heats the initial portion of the fiber, whereas the remaining portion is subjected to cooling.

**3.1.  $\ell = 1$ .** Introducing the scaled effective force  $\mathcal{F} = 2Fe^{\alpha_\mu}/\ln D_r$ , we can rewrite the system (2.24) and (2.25) as

$$(3.1) \quad s_z = -\mathcal{F} \ln D_r s e^{-\alpha_\mu(1-\theta)},$$

$$(3.2) \quad \theta_z = \mathcal{H}_f \sqrt{s}(1-\theta),$$

subject to the boundary conditions  $s(0) = 1$  and  $\theta(0) = 0$ . From the above two equations, we obtain

$$(3.3) \quad \frac{ds}{d\theta} = -\frac{\mathcal{F} \ln D_r}{\mathcal{H}_f} \frac{\sqrt{s} e^{-\alpha_\mu(1-\theta)}}{1-\theta}.$$

Integrating and using the boundary conditions, we obtain

$$(3.4) \quad s = \left( 1 - \frac{\mathcal{F} \ln D_r}{2\mathcal{H}_f} \{E_1[\alpha_\mu(1-\theta)] - E_1[\alpha_\mu]\} \right)^2$$

where

$$E_1[\eta] = \int_\eta^\infty \frac{e^{-x}}{x} dx$$

is the exponential integral. Note that up to this point no approximation has been made to (3.1) and (3.2). To proceed further, we exploit the fact that viscosity varies rapidly with temperature, that is,  $\alpha_\mu \gg 1$ . Note that the exponential integral has the following asymptotic approximations:

$$E_1[\eta] \sim \frac{e^{-\eta}}{\eta} \text{ as } \eta \rightarrow \infty, \quad E_1[\eta] \sim -\ln(\eta) - \gamma \text{ as } \eta \rightarrow 0$$

where  $\gamma = 0.5772\dots$  is Euler's constant.

From (3.2), we have

$$(3.5) \quad \theta_z = \mathcal{H}_f \left( 1 - \frac{\mathcal{F} \ln D_r}{2\mathcal{H}_f} \{E_1[\alpha_\mu(1-\theta)] - E_1[\alpha_\mu]\} \right) (1-\theta).$$

Since  $\alpha_\mu \approx 30 \gg 1$ , we have that  $E_1[\alpha_\mu]$  is small. Also,  $E_1[\alpha_\mu(1-\theta)]$  will be small if  $1-\theta \gg \alpha_\mu^{-1}$ . Therefore,

$$(3.6) \quad \theta_z = \mathcal{H}_f(1-\theta),$$

which can be solved to give

$$(3.7) \quad \theta = 1 - e^{-\mathcal{H}_f z}.$$

Clearly,  $1-\theta \rightarrow 0$  as  $z$  increases to 1 for  $\mathcal{H}_f \gg 1$ . Thus, for  $z \gg \mathcal{H}_f^{-1}$ , we have

$$(3.8) \quad \theta_z = \mathcal{H}_f \left( 1 + \frac{\mathcal{F} \ln D_r}{2\mathcal{H}_f} \{\ln[\alpha_\mu(1-\theta)] + \gamma\} \right) (1-\theta).$$

Letting

$$\alpha_\mu(1 - \theta) = e^{-\frac{2\mathcal{H}_f}{\mathcal{F} \ln D_r} \hat{\theta}},$$

we have

$$(3.9) \quad \hat{\theta}_z = -\frac{\mathcal{F} \ln D_r}{2} (\ln \hat{\theta} + \gamma) \hat{\theta},$$

which can be integrated to obtain

$$(3.10) \quad \ln \hat{\theta} = -\gamma + C_1 e^{-\frac{\mathcal{F} \ln D_r}{2} z}$$

where  $C_1$  is an integration constant.

Next, we match the above solution with (3.6) to obtain

$$(3.11) \quad C_1 = \gamma + \ln \alpha_\mu + \frac{2\mathcal{H}_f}{\mathcal{F} \ln D_r}.$$

Thus,

$$(3.12) \quad \hat{\theta} = \exp \left[ -\gamma + \left( \gamma + \ln \alpha_\mu + \frac{2\mathcal{H}_f}{\mathcal{F} \ln D_r} \right) e^{-\frac{\mathcal{F} \ln D_r}{2} z} \right],$$

or returning to the original variable,

$$(3.13) \quad \theta = 1 - \exp \left[ - \left( \gamma + \ln \alpha_\mu + \frac{2\mathcal{H}_f}{\mathcal{F} \ln D_r} \right) \left( 1 - e^{-\frac{\mathcal{F} \ln D_r}{2} z} \right) \right].$$

Given  $\theta$ , we can find  $s$  using (3.4).

The scaled pulling force  $\mathcal{F}$  can be obtained by substituting  $z = 1$  into (3.13) and (3.4) and using the condition  $s(1) = D_r^{-1}$ . Using the fact that  $\alpha_\mu \gg 1$  and the asymptotic properties of  $E_1$ , we obtain

$$(3.14) \quad \mathcal{F} = 1 + \frac{2}{\ln D_r} \ln \left[ 1 + \frac{\mathcal{F}(\ln \alpha_\mu + \gamma) \ln D_r}{2\mathcal{H}_f} \right].$$

In general, to obtain  $\mathcal{F}$ , this equation must be solved numerically. But for typical parameter values, we have

$$(3.15) \quad \frac{(\ln \alpha_\mu + \gamma) \ln D_r}{2\mathcal{H}_f} \sim 10^{-1} \ll 1,$$

and so we can obtain an asymptotic estimate for  $\mathcal{F}$  in closed form:

$$(3.16) \quad \mathcal{F} = 1 + \frac{\ln \alpha_\mu + \gamma}{\mathcal{H}_f}.$$

In Figure 2, we plot the asymptotic and numerical solutions, and it can be seen that the agreement between the two solutions is excellent.

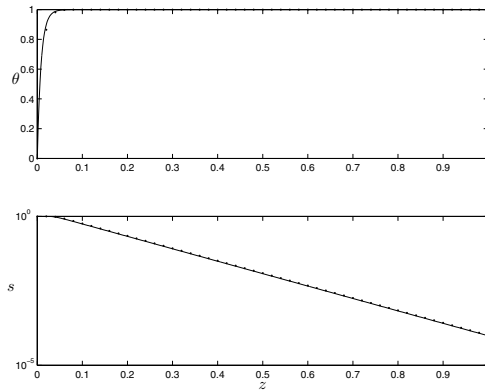


FIG. 2. Numerical (dots) vs. asymptotic (lines) solutions. The parameter values are  $\mathcal{H}_f = 100$ ,  $\alpha_\mu = 30$ , and  $D_r = 10^4$ .

**3.2.  $\ell < 1$ .** When there is cooling, the previous solution is valid up to the location  $z = \ell$ , but for  $z > \ell$ , the area and temperature are determined from (2.24) and (2.25):

$$(3.17) \quad s_z = -\mathcal{F} \ln(D_r) e^{\alpha_\mu(\theta-1)} s,$$

$$(3.18) \quad \theta_z = -\mathcal{H}_c \sqrt{s} \theta,$$

subject to the boundary conditions  $s(\ell) = s_\ell$  and  $\theta(\ell) = \theta_\ell$ .

We rescale the variables using

$$\vartheta = \alpha_\mu(\theta_\ell - \theta), \quad \mathfrak{s} = \sqrt{\frac{s}{s_\ell}}, \quad y = \frac{\mathcal{F} \ln(D_r) e^{\alpha_\mu(\theta_\ell-1)}}{2} (z - \ell),$$

and (3.17) and (3.18) become

$$(3.19) \quad \mathfrak{s}_y = -\mathfrak{s} e^{-\vartheta},$$

$$(3.20) \quad \vartheta_y = \mathcal{A} \mathfrak{s} (1 - \epsilon \vartheta)$$

where

$$\mathcal{A} = \frac{2\sqrt{s_\ell} \mathcal{H}_c \alpha_\mu \theta_\ell e^{\alpha_\mu(1-\theta_\ell)}}{\mathcal{F} \ln(D_r)}, \quad \epsilon = \frac{1}{\alpha_\mu \theta_\ell} \ll 1,$$

and subject to  $\vartheta(0) = 0$  and  $\mathfrak{s}(0) = 1$ .

From (3.19) and (3.20), we obtain

$$(3.21) \quad \frac{d\vartheta}{d\mathfrak{s}} = -\mathcal{A}(1 - \epsilon\vartheta)e^\vartheta.$$

Using  $\vartheta(0) = 0$ ,  $\mathfrak{s}(0) = 1$ , and integration by parts, we obtain

$$(3.22) \quad \mathfrak{s} = 1 - \frac{1}{\mathcal{A}} \int_0^\vartheta \frac{e^{-w}}{1 - \epsilon w} dw = 1 + \frac{1}{\mathcal{A}} \left( \frac{e^{-\vartheta}}{1 - \epsilon\vartheta} - 1 \right) - \frac{\epsilon}{\mathcal{A}} \int_0^\vartheta \frac{e^{-w}}{(1 - \epsilon w)^2} dw.$$

Given typical parameter values, one can readily see that the scaled temperature  $\vartheta$  at the exit is much greater than  $\epsilon^{-1}$ . Therefore,  $\epsilon/(1 - \epsilon\vartheta) \ll 1$ , and (3.22) can be

approximated as

$$(3.23) \quad \mathfrak{s} = 1 + \frac{1}{\mathcal{A}} \left( \frac{e^{-\vartheta}}{1 - \epsilon\vartheta} - 1 \right).$$

We now proceed with three different cases:  $\mathcal{A} = 1$ ,  $\mathcal{A} < 1$ , and  $\mathcal{A} > 1$ .

**Case 1.  $\mathcal{A} = 1$ .** In this case, we have

$$(3.24) \quad \mathfrak{s} = e^{-\vartheta}$$

and the equation for  $\vartheta$  becomes

$$(3.25) \quad \vartheta_y = e^{-\vartheta},$$

which can be solved as

$$(3.26) \quad \vartheta = \ln(y + 1)$$

using the boundary condition  $\vartheta(0) = 0$ . Thus, the leading-order solution for  $\mathfrak{s}$  is

$$(3.27) \quad \mathfrak{s} = \frac{1}{(y + 1)}.$$

**Case 2.  $\mathcal{A} < 1$ .** Note that  $\mathcal{A}$  is the scaled cooling strength, and when  $\mathcal{A} < 1$ , we expect that the temperature is bounded below by  $\mathcal{A} = 1$ . Using the solution in Case 1, we note that  $\vartheta$  is a monotonically increasing function with a maximum value

$$(3.28) \quad \vartheta_{max} = \ln \left( \frac{\mathcal{F} \ln(D_r) e^{\alpha\mu(\theta_\ell - 1)}}{2} (1 - \ell) + 1 \right).$$

The quantity  $\vartheta_{max}$  is an order one quantity as long as  $\ln(\ln(D_r)) \ll \epsilon^{-1}$ , so we conclude that  $\vartheta$  also will be an order one quantity.

Having established that  $\vartheta = O(1)$ , we can approximate (3.23) by

$$(3.29) \quad \mathfrak{s} = 1 + \frac{1}{\mathcal{A}} (e^{-\vartheta} - 1).$$

From (3.20), we obtain

$$(3.30) \quad \vartheta_y = \mathcal{A}\mathfrak{s} = e^{-\vartheta} + \mathcal{A} - 1,$$

which can be integrated to give

$$(3.31) \quad \vartheta = \ln \frac{\mathcal{A}e^{(\mathcal{A}-1)y} - 1}{\mathcal{A} - 1}$$

after applying the condition  $\vartheta(0) = 0$ . Note that this solution also applies to the case of  $\mathcal{A} = 1$  by taking the limit  $\mathcal{A} \rightarrow 1$ , which yields (3.26). The solution for  $\mathfrak{s}$  can be obtained as

$$(3.32) \quad \mathfrak{s} = \frac{\mathcal{A} - 1}{\mathcal{A} - e^{-(\mathcal{A}-1)y}}.$$

**Case 3.  $\mathcal{A} > 1$ .** In this case, we need to consider two scenarios: when  $\vartheta = O(1)$  and when  $\vartheta$  is large.

(i)  $\vartheta = O(1)$ . When  $\vartheta = O(1)$ , the analysis is identical to the case for  $\mathcal{A} < 1$ , yielding the same formulas (3.31) and (3.32).

(ii) *Large  $\vartheta$ .* When  $1 \ll \vartheta \ll \epsilon^{-1}$  and  $\mathcal{A} > 1$ , the approximation of (3.23), neglecting exponentially small terms, is given by

$$(3.33) \quad \mathfrak{s} = 1 - \frac{1}{\mathcal{A}},$$

which can be combined with (3.20) to yield

$$(3.34) \quad \vartheta_y = (\mathcal{A} - 1)(1 - \epsilon\vartheta).$$

This equation can be solved as

$$(3.35) \quad \vartheta = \frac{1 - C_2 e^{-\epsilon(\mathcal{A}-1)y}}{\epsilon}$$

where  $C_2$  is an integration constant. Since we obtained the solution based on the assumption that  $\vartheta$  is not small, we cannot use the boundary condition  $\vartheta(0) = 0$ . To determine  $C_2$ , we need to match the small  $\vartheta$  solution given by (3.31) with that for large  $\vartheta$  given by (3.35). Taking the limit of  $\vartheta \rightarrow 0$  from (3.35), we obtain

$$\vartheta \sim \frac{1 - C_2(1 - \epsilon(\mathcal{A} - 1)y)}{\epsilon}.$$

For large  $\vartheta$ , i.e.,  $y \rightarrow 0$ , (3.31) gives

$$\vartheta \sim (\mathcal{A} - 1)y + \ln \frac{\mathcal{A}}{\mathcal{A} - 1}.$$

Comparing the two expressions, the only choice we have is

$$C_2 = 1 - \epsilon \ln \frac{\mathcal{A}}{\mathcal{A} - 1},$$

and the solution becomes

$$(3.36) \quad \vartheta = \frac{1 - e^{-\epsilon(\mathcal{A}-1)y}}{\epsilon} + \left( \ln \frac{\mathcal{A}}{\mathcal{A} - 1} \right) e^{-\epsilon(\mathcal{A}-1)y}.$$

Note that when  $\mathcal{A} \gg 1$ ,  $C_2 \sim 1$  and  $\vartheta$  can be approximated by

$$(3.37) \quad \vartheta = \frac{1 - e^{-\epsilon(\mathcal{A}-1)y}}{\epsilon}.$$

(iii) *Uniformly valid solution.* The uniformly valid solution for  $\vartheta$  obtained by combining the solutions for small and large values of  $\vartheta$  is given by

$$(3.38) \quad \vartheta = \ln \frac{\mathcal{A}e^{(\mathcal{A}-1)y} - 1}{\mathcal{A} - 1} + \frac{1 - e^{-\epsilon(\mathcal{A}-1)y}}{\epsilon} + \ln \frac{\mathcal{A}}{\mathcal{A} - 1} e^{-\epsilon(\mathcal{A}-1)y} - (\mathcal{A} - 1)y - \ln \frac{\mathcal{A}}{\mathcal{A} - 1}.$$

The solution for  $\mathfrak{s}$  can be obtained using (3.23).

**Solutions in original variables.** Using the original variables and  $\theta = \theta_\ell - \alpha_\mu^{-1}\vartheta$ , the temperature solution is given by

$$(3.39) \quad \theta = \theta_\ell - \frac{1}{\alpha_\mu} \ln \frac{\mathcal{A} \exp[(\mathcal{A} - 1)\mathcal{B}(z - \ell)] - 1}{\mathcal{A} - 1}$$

for  $\mathcal{A} \leq 1$  and

$$(3.40) \quad \begin{aligned} \theta = \theta_\ell - \frac{1}{\alpha_\mu} \ln \frac{\mathcal{A} \exp[(\mathcal{A} - 1)\mathcal{B}(z - \ell)] - 1}{\mathcal{A} - 1} \\ - \left( \theta_\ell - \frac{1}{\alpha_\mu} \ln \frac{\mathcal{A}}{\mathcal{A} - 1} \right) \left( 1 - \exp \left[ -\frac{(\mathcal{A} - 1)\mathcal{B}}{\alpha_\mu \theta_\ell} (z - \ell) \right] \right) + \frac{1}{\alpha_\mu} (\mathcal{A} - 1)\mathcal{B}(z - \ell) \end{aligned}$$

for  $\mathcal{A} > 1$ . Here  $\mathcal{B} = \mathcal{F} \ln(D_r) e^{\alpha_\mu(\theta_\ell - 1)}/2$ .

In both cases, the solution for the cross-sectional area in the original variables is obtained using (3.23):

$$(3.41) \quad s = s_\ell \left( 1 - \frac{1}{\mathcal{A}} + \frac{\theta_\ell \exp[\alpha_\mu(\theta - \theta_\ell)]}{\mathcal{A}\theta} \right)^2.$$

Using  $s(1) = D_r^{-1}$ , we can obtain  $\mathcal{F}$  (and  $F$ ) by solving the following equation numerically:

$$(3.42) \quad D_r^{-1} = s_\ell \left( 1 - \frac{1}{\mathcal{A}} + \frac{\theta_\ell \exp[\alpha_\mu(\theta(1) - \theta_\ell)]}{\mathcal{A}\theta(1)} \right)^2$$

where  $\theta(1)$  is evaluated at  $z = 1$  using (3.39) or (3.40), depending on the value of  $\mathcal{A}$ .

In Figures 3 and 4, we have plotted both the numerical and the asymptotic solutions for various values of the draw ratio  $D_r$  and for two different values of the cooling parameter  $\mathcal{H}_c$ , respectively. It can be seen that the solutions agree very well with each other. Therefore, instead of relying on numerical solutions, one can use (3.39) and (3.40) to evaluate the effective diffusion coefficient for the dopant. This will be shown in the next section.

**4. Dopant diffusion.** Since dopant transport follows a standard diffusion equation, the solution is completely determined by the effective diffusion coefficient. When the diffusion coefficient is small (as in the case of dopant diffusion), the effect of the boundary on the dopant distribution is also small. Therefore, we can ignore the boundary and solve (2.29) on an infinite domain as an approximation.<sup>2</sup> In this case, the solution for the dopant concentration can be written as

$$(4.1) \quad c(\tau, \xi) = 2\pi \int_0^1 G(\tau, \xi; \eta) c_0(\eta) \eta d\eta.$$

<sup>2</sup>If we consider the boundary effect, we can use the series solution given by

$$c(\tau, \xi) = 2 \left[ 1 + \frac{r^*}{R} \sum_{m=1}^{\infty} e^{-\lambda_m^2 \mathcal{D}\tau} \frac{J_0(\lambda_m \xi) J_1(\lambda_m r^* R^{-1})}{\lambda_m J_0(\lambda_m)^2} \right]$$

where  $\lambda_m$  are the zeros of  $J_1(\lambda)$ . As long as the diffusion is not too small, only a small number of terms is needed. For small diffusion coefficient values, convergence becomes slow, and we can switch to the solution based on the infinite domain Green's function.

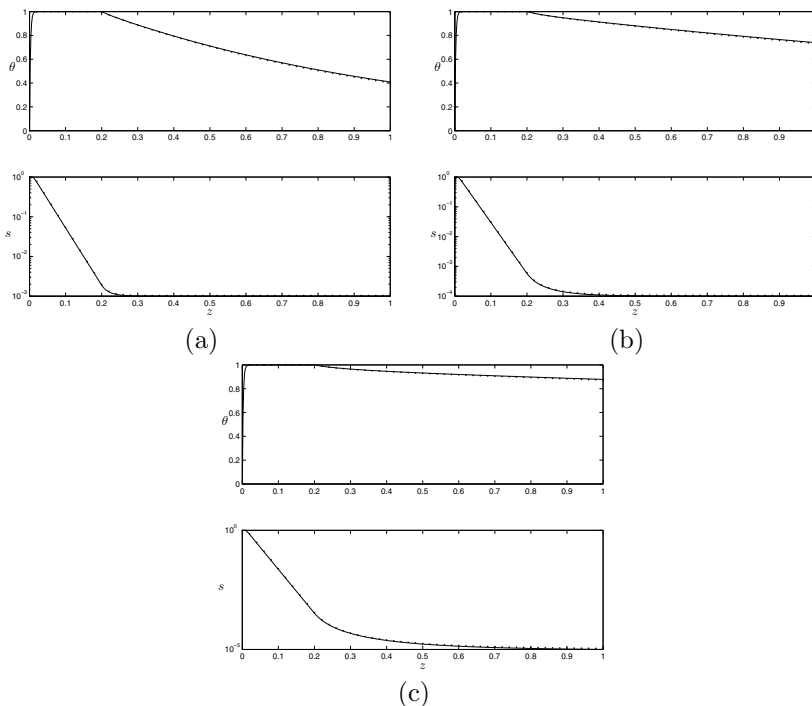


FIG. 3. Numerical (dots) vs. asymptotic solutions (solid line) given by (3.40) and (3.41): (a)  $D_r = 10^3$  ( $\mathcal{A} = 3.67$ ); (b)  $D_r = 10^4$  ( $\mathcal{A} = 1.71$ ); and (c)  $D_r = 10^5$  ( $\mathcal{A} = 1.20$ ). Values of the other parameters are  $\mathcal{H} = 350$ ,  $\mathcal{H}_c = 35$ ,  $\alpha_\mu = 40$ ,  $\ell = 0.2$ .

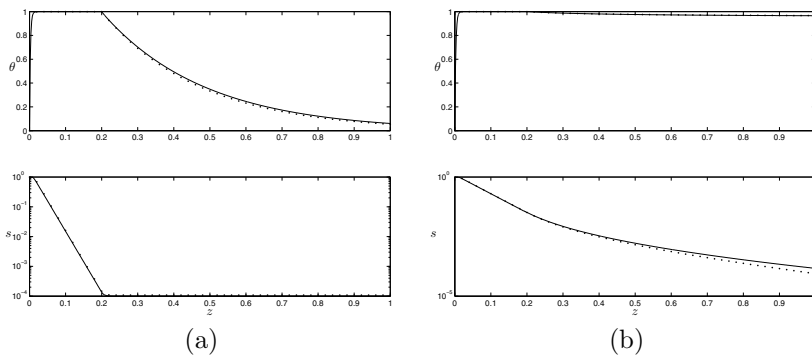


FIG. 4. Numerical (dots) vs. asymptotic solutions (solid line) given by (3.39), (3.40), and (3.41): (a)  $\mathcal{H}_c = 350$  ( $\mathcal{A} = 6.96$ ); and (b)  $\mathcal{H}_c = 1$  ( $\mathcal{A} = 0.78$ ). Values of the other parameters are  $\mathcal{H} = 350$ ,  $D_r = 10^4$ ,  $\alpha_\mu = 40$ ,  $\ell = 0.2$ .

If we know the value of  $\mathcal{D}$ , then the Green's function is given by

$$(4.2) \quad G(\tau, \xi; \eta) = \frac{1}{4\pi\mathcal{D}\tau} \exp\left(-\frac{\xi^2 + \eta^2}{4\mathcal{D}\tau}\right) I_0\left(\frac{\xi\eta}{2\mathcal{D}\tau}\right)$$

where  $I_0$  is the modified Bessel function of the first kind.

In order to illustrate how the effective diffusion coefficient  $\mathcal{D}$  is affected by various parameter values, we obtain an asymptotic approximation for the case with no cooling



( $\ell = 1$ ). Recall that in this case, the temperature is given by (3.13):

$$\theta = 1 - \exp \left[ -C_1 \left( 1 - e^{-\frac{\mathcal{F} \ln D_r}{2} z} \right) \right],$$

with  $C_1$  given by (3.11) and the effective diffusion coefficient is given by  $\mathcal{D} = \bar{\phi}/\mathcal{P}$  where  $\bar{\phi}$  is given by (2.27) with  $D$  given by (2.20).

Introducing new variables  $\zeta = 1 - \exp(-\frac{\mathcal{F} \ln D_r}{2} z)$  and  $\varphi(\zeta) \equiv \phi(z)$ , we have

$$d\zeta = \frac{\mathcal{F} \ln D_r}{2} (1 - \zeta) dz$$

and

$$(4.3) \quad \varphi_\zeta = \frac{2}{\mathcal{F} \ln D_r} \frac{\exp\left(-\frac{\alpha_D}{\Theta+1-\exp(-C_1\zeta)}\right)}{1-\zeta}, \quad \varphi(0) = 0.$$

Since  $C_1 \gg 1$ , the solution can be found for two cases:  $\zeta \sim C_1^{-1}$  and  $\zeta \sim 1$ .

**Case I.**  $\zeta \sim C_1^{-1} \ll 1$ . In this case, we use a new variable  $\hat{\zeta} = C_1\zeta$  and denote the solution by  $\varphi^{(i)}$  (inner solution) which satisfies

$$(4.4) \quad \varphi_{\hat{\zeta}}^{(i)} = \frac{2 \exp\left(-\frac{\alpha_D}{\Theta+1-\exp(-\hat{\zeta})}\right)}{C_1 \mathcal{F} \ln D_r}, \quad \varphi^{(i)}(0) = 0.$$

The inner solution can be obtained as

$$(4.5) \quad \varphi^{(i)}(\hat{\zeta}) = -\frac{2}{C_1 \mathcal{F} \ln D_r} \left[ E_1(x) - \exp\left(-\frac{\alpha_D}{\Theta+1}\right) E_1\left(x - \frac{\alpha_D}{\Theta+1}\right) \right]_{x=\alpha_D/\Theta}^{x=\alpha_D/(\Theta+1-\exp(-\hat{\zeta}))}.$$

**Case II.**  $\zeta \sim 1$ . In this case, we denote the solution by  $\varphi^{(o)}$  (outer solution) which satisfies

$$(4.6) \quad \varphi_\zeta^{(o)} = \frac{2}{\mathcal{F} \ln D_r} \frac{\exp(-\frac{\alpha_D}{\Theta+1})}{1-\zeta}.$$

The solution can be obtained as

$$(4.7) \quad \varphi^{(o)}(\zeta) = -\frac{2 \exp(-\frac{\alpha_D}{\Theta+1})}{\mathcal{F} \ln D_r} \ln(1-\zeta) + C_3$$

where  $C_3$  is an integration constant.

**Matching.** To determine the integration constant  $C_3$  and the outer solution,  $\varphi^{(o)}$ , we need to match the two solutions as follows:

$$\lim_{\hat{\zeta} \rightarrow \infty} \varphi^{(i)}(\hat{\zeta}) = \lim_{\zeta \rightarrow 0} \varphi^{(o)}(\zeta).$$

Since

$$(4.8) \quad \varphi^{(o)}(\zeta) \sim C_3 + \frac{2 \exp(-\frac{\alpha_D}{\Theta+1})}{\mathcal{F} \ln D_r} \zeta \quad \text{as } \zeta \rightarrow 0$$

and  $E_1[z] \sim -\gamma - \ln(z)$  for small  $z$ , we have

$$\begin{aligned}
 \varphi^{(i)}(\hat{\zeta}) &\sim -\frac{2}{C_1 \mathcal{F} \ln D_r} \left\{ E_1\left(\frac{\alpha_D}{\Theta+1}\right) - E_1\left(\frac{\alpha_D}{\Theta}\right) - \exp\left(-\frac{\alpha_D}{\Theta+1}\right) \right. \\
 &\quad \times \left[ -\gamma - \ln\left(\frac{\alpha_D}{\Theta+1 - \exp(-\hat{\zeta})} - \frac{\alpha_D}{\Theta+1}\right) \right] \\
 &\quad \left. + \exp\left(-\frac{\alpha_D}{\Theta+1}\right) E_1\left(\frac{\alpha_D}{\Theta} - \frac{\alpha_D}{\Theta+1}\right) \right\} \\
 &\approx -\frac{2}{C_1 \mathcal{F} \ln D_r} \left\{ E_1\left(\frac{\alpha_D}{\Theta+1}\right) - E_1\left(\frac{\alpha_D}{\Theta}\right) - \exp\left(-\frac{\alpha_D}{\Theta+1}\right) \right. \\
 &\quad \times \left[ -\gamma - \ln \alpha_D + \hat{\zeta} + 2 \ln(\Theta+1) \right] + \exp\left(-\frac{\alpha_D}{\Theta+1}\right) E_1\left(\frac{\alpha_D}{\Theta(\Theta+1)}\right) \left. \right\} \\
 &\approx -\frac{2}{C_1 \mathcal{F} \ln D_r} \left\{ E_1\left(\frac{\alpha_D}{\Theta+1}\right) - E_1\left(\frac{\alpha_D}{\Theta}\right) - \exp\left(-\frac{\alpha_D}{\Theta+1}\right) \right. \\
 &\quad \times \left[ -\gamma - \ln \alpha_D + 2 \ln(\Theta+1) \right] + \exp\left(-\frac{\alpha_D}{\Theta+1}\right) E_1\left(\frac{\alpha_D}{\Theta(\Theta+1)}\right) \left. \right\} \\
 (4.9) \quad &+ \frac{2 \exp\left(-\frac{\alpha_D}{\Theta+1}\right)}{\mathcal{F} \ln D_r} \frac{\hat{\zeta}}{C_1} \quad \text{as } \hat{\zeta} \rightarrow \infty.
 \end{aligned}$$

We obtain

$$\begin{aligned}
 C_3 &= -\frac{2}{C_1 \mathcal{F} \ln D_r} \left\{ E_1\left(\frac{\alpha_D}{\Theta+1}\right) - E_1\left(\frac{\alpha_D}{\Theta}\right) - \exp\left(-\frac{\alpha_D}{\Theta+1}\right) \right. \\
 (4.10) \quad &\quad \left. \times \left[ -\gamma - \ln \alpha_D + 2 \ln(\Theta+1) \right] + \exp\left(-\frac{\alpha_D}{\Theta+1}\right) E_1\left(\frac{\alpha_D}{\Theta(\Theta+1)}\right) \right\}.
 \end{aligned}$$

Using the original variable, we have

$$(4.11) \quad \phi^{(o)}(z) = \exp\left(-\frac{\alpha_D}{\Theta+1}\right) z + C_3,$$

from which we obtain the effective diffusion coefficient as

$$(4.12) \quad \mathcal{D} = \frac{\exp\left(-\frac{\alpha_D}{\Theta+1}\right) + C_3}{\mathcal{P}}.$$

First, we observe that the first term on the right-hand side of  $\mathcal{D}$  is given by  $\mathcal{P}^{-1} \exp\left(-\frac{\alpha_D}{\Theta+1}\right)$ , which is the value of the effective diffusion coefficient when  $\theta = \Theta$  for all  $z$ , i.e., uniform temperature. The correction term  $C_3$  is inversely proportional to

$$2\mathcal{H}_f + (\ln \alpha_\mu + \gamma) \left( 1 + \frac{\ln \alpha_\mu + \gamma}{\mathcal{H}_f} \right) \ln D_r.$$

The parameter  $\mathcal{H}_f$  is typically much larger than the other parameters. Therefore, the above asymptotic analysis clearly shows that the effective diffusion is extremely weakly dependent on the draw ratio  $D_r$ .

On the other hand,  $\mathcal{D}$  is strongly affected by the Péclet number  $\mathcal{P}$ . Therefore, the most effective way to control excessive diffusion is to increase  $\mathcal{P}$ , which can be achieved by using a relatively large feeding speed. We note that the diffusion coefficient given here is for the scaled fiber radius. Thus, the absolute length of diffusion is proportional to the initial fiber radius  $R_0$ . For illustrative purposes, we have evaluated the effective diffusion coefficient given in (4.12) using the parameter values listed in Table 1 and keeping the feeding speed as a free parameter, yielding

$$\mathcal{D} \approx \frac{3.02 \times 10^{-9}}{u_0} - \frac{1.44 \times 10^{-11}}{4.27u_0^2 + 5.10 \times 10^{-5}} \text{ m}^2/\text{s}.$$

Here the second term comes from the correction term  $C_3/\mathcal{P}$ . Taking the value of  $u_0 = 10^{-4}$  m/s (cf. [6]), we obtain  $\mathcal{D} \approx 2.99 \times 10^{-5}$  m<sup>2</sup>/s with the correction term and  $3.02 \times 10^{-5}$  m<sup>2</sup>/s without the correction term. Next we compute the effective diffusion coefficient using numerical quadrature, based on (2.27), (2.28), and (3.13), which yields  $\mathcal{D} = 2.99 \times 10^{-5}$  m<sup>2</sup>/s. For a higher feeding speed, e.g.,  $u_0 = 3 \times 10^{-3}$  m/s, the asymptotic solution is  $\mathcal{D} \approx 8.45 \times 10^{-7}$  m<sup>2</sup>/s with the correction term and  $1.01 \times 10^{-6}$  m<sup>2</sup>/s without the correction term, while the numerical solution is  $\mathcal{D} = 8.5 \times 10^{-7}$  m<sup>2</sup>/s. In both cases the asymptotic solution is a very good approximation when it is compared with the numerical solution, especially when the correction term is included.

Finally, to find  $\mathcal{D}$  for the case with cooling, we could solve for the temperature from (2.24)–(2.25) with boundary condition (2.26). The effective diffusion coefficient could be computed using the integral  $\int_0^1 D(\theta) dz$ . In general, we can apply numerical methods, e.g., finite difference to solve the flow and temperature equations (2.24) and (2.25) and numerical quadrature to the integral to find an approximation of  $\mathcal{D}$ . However, since we already obtained an asymptotic solution for the temperature,  $\mathcal{D}$  can be computed easily by evaluating the integral using numerical quadrature.

**5. Conclusion.** In this paper, we have shown that the long-wave approximation can be used to dramatically simplify the governing equations for dopant transport in optical fiber drawing. The viscosity and diffusion coefficient vary rapidly with temperature, which makes direct numerical simulations difficult. However, we take advantage of these rapid changes to derive asymptotic approximations of the solution. We show that the transport of dopant satisfies a simple diffusion equation with an effective diffusion coefficient that can be computed easily using our asymptotic solution. Our solution shows that the feeding speed is the most effective way to control dopant diffusion from the core into the cladding region. Using our asymptotic solution, other control strategies can also be developed. For example, one can use an optimal control framework based on a cost function that maximizes fiber production and minimizes dopant diffusion and which uses the feeding and drawing speeds or the heating and cooling rates as control variables. However, such a study is beyond the scope of this paper and will be pursued in future work.

#### REFERENCES

- [1] A. D. FITT, K. FURUSAWA, T. M. MONRO, AND C. P. PLEASE, *Modeling the fabrication of hollow fibers: Capillary drawing*, *J. Lightwave Technol.*, 19 (2001), pp. 1924–1931.
- [2] G. GUPTA AND W. W. SCHULTZ, *Non-isothermal flows of Newtonian slender glass fibers*, *Internat. J. Non-Linear Mech.*, 33 (1998), pp. 151–163.

- [3] H. HUANG, R. M. MIURA, W. P. IRELAND, AND E. PUIL, *Heat-induced stretching of a glass tube under tension: Application to glass microelectrodes*, SIAM J. Appl. Math., 63 (2003), pp. 1499–1519.
- [4] T. IZAWA, *Early days of VAD process*, IEEE J. Selected Topics Quantum Electronics, 6 (2000), pp. 1220–1227.
- [5] K. LYYTIKÄINEN, S. T. HUNTINGTON, A. L. G. CARTER, P. MCNAMARA, S. FLEMING, J. ABRAMCZYK, I. KAPLIN, AND G. SCHÖTZ, *Dopant diffusion during optical fibre drawing*, Optical Express, 12 (2004), pp. 972–977.
- [6] S. H.-K. LEE AND Y. JALURIA, *Effects of variable properties and viscosity dissipation during optical fiber drawing*, Trans. ASME, 118 (1996), pp. 350–358.
- [7] E. PONE, X. DAXHELET, AND S. LACROIX, *Refractive index profile of fused-fiber couplers cross-section*, Optical Express, 12 (2004), pp. 1036–1044.
- [8] H. SCHOLZE, *Glass, Nature, Structure, and Properties*, M. J. Lakin, trans., Springer-Verlag, New York, 1990, pp. 255–272.
- [9] J. WYLIE AND H. HUANG, *Extensional flows with viscous heating*, J. Fluid Mech., 570 (2007), pp. 359–370.
- [10] J. WYLIE, H. HUANG, AND R. M. MIURA, *Thermal instability in drawing viscous threads*, J. Fluid Mech., 570 (2007), pp. 1–13.
- [11] Y. YAN AND R. PITCHUMANI, *Numerical study on the dopant concentration and refractive index profile evolution in an optical fiber manufacturing process*, Int. J. Heat Mass Transfer, 49 (2006), pp. 2097–2112.